PHILOSOPHICAL TRANSACTIONS OF THE ROYAL SOCIETY A MATHEMATICAL, PHYSICAL & ENGINEERING SCIENCES

The Effect of Flow Unsteadiness on the Homogeneous Nucleation of Water Droplets in Steam Turbines

Abhijit Guha and John Young

Phil. Trans. R. Soc. Lond. A 1994 **349**, 445-472
doi: 10.1098/rsta.1994.0141

The effect of flow unsteadiness on the homogeneous nucleation of water droplets in steam turbines

By Abhijit Guha[1] and John Young[2]

[1] *Gonville and Caius College, Cambridge University, Cambridge CB2 1TA, U.K.*
[2] *Whittle Laboratory, Department of Engineering, University of Cambridge, Madingley Road, Cambridge CB3 0DY, U.K.*

The paper describes a new theory of the formation and growth of water droplets in multistage steam turbines. The essence of the theory is that large-scale static temperature fluctuations caused by the segmentation of blade wakes by successive blade rows have a dominating influence on nucleation and droplet growth in turbines. 'True' turbulent fluctuations (due to shear-layer unsteadiness, etc.) are probably less important and are ignored. A Lagrangian frame of reference is adopted and attention is focused on a large number of individual fluid particles during their passage through the turbine. Homogeneous nucleation and growth of droplets in each fluid particle is assumed to be governed by classical theories. All fluid particles are assumed to experience the same pressure variation, but those particles passing close to the blade surfaces suffer greater entropy production and, therefore, have higher static temperatures than those that pursue nearly isentropic paths through the central portions of the blade passages. Particles which suffer high loss therefore nucleate later in the turbine than those that experience little dissipation. Condensation is thus viewed as an essentially random and unsteady phenomenon because the dissipation experienced by a fluid particle in one blade row is assumed to be uncorrelated with its previous history. On a time-averaged basis, the condensation zone is spread over a much greater distance in the flow direction than a simple steady-flow analysis would indicate and may encompass several blade rows, depending on the number of stages in the machine. Predicted droplet size spectra show broad, highly skewed distributions with large mean diameters and sometimes slight bimodality. These are all characteristics of experimentally measured spectra in real turbines. Conventional, steady-flow calculation methods, which predict a fixed Wilson point in a specific blade row and a nearly monodispersed droplet population, cannot reproduce any of these characteristics.

Nomenclature

Scalar quantities:

c_p	isobaric specific heat capacity
h	specific enthalpy
h_0	relative stagnation specific enthalpy
I	specific rothalpy
k	thermal conductivity

Phil. Trans. R. Soc. Lond. A (1994) **349**, 445–472
Printed in Great Britain

k_t	turbulent thermal conductivity
L	axial chord length
m	mass of a droplet
n	number of droplets per unit mass of mixture
p	pressure
Re	Reynolds number
r	droplet radius
s	specific entropy
T	temperature
ΔT	vapour subcooling
ΔT_{cap}	capillary subcooling
t	time
y	wetness fraction
δ	wake thickness
Φ	dissipation function
η	polytropic efficiency
λ	second viscosity
μ	dynamic viscosity
μ_t	turbulent dynamic viscosity
ρ	density
τ_E	wake equilibration time
τ_T	two-phase thermal relaxation time
ξ	Markov loss coefficient

Vector (bold) and tensor quantities

$\boldsymbol{w}$	relative velocity
$\boldsymbol{q}$	heat flux
$\boldsymbol{q}_t$	turbulent heat flux
$\boldsymbol{r}$	position vector
$\boldsymbol{\Omega}$	angular velocity
σ	viscous stress tensor
σ_t	Reynolds stress tensor

Subscripts, etc:

A	aerodynamic
i	droplet group i
is	isentropic
s	saturated
v	vapour phase
$\bar{}$	Reynolds-averaged quantity
$\tilde{}$	Favre-averaged quantity

1. Introduction

One of the major unsolved problems in the themo-fluid-dynamic theory of wet-steam turbines is the prediction of the formation and growth of liquid-phase droplets from the supersaturated vapour formed by the rapid expansion of the steam within the blade passages. This lack of understanding is a serious obstacle when assessing the effects of departures from equilibrium on the flow behaviour, the magnitude of the wetness loss and the rate of fog droplet deposition on the blading. The quantitative evaluation of all these phenomena requires a knowledge of the size distribution of fog

PHILOSOPHICAL TRANSACTIONS OF THE ROYAL SOCIETY A MATHEMATICAL, PHYSICAL & ENGINEERING SCIENCES

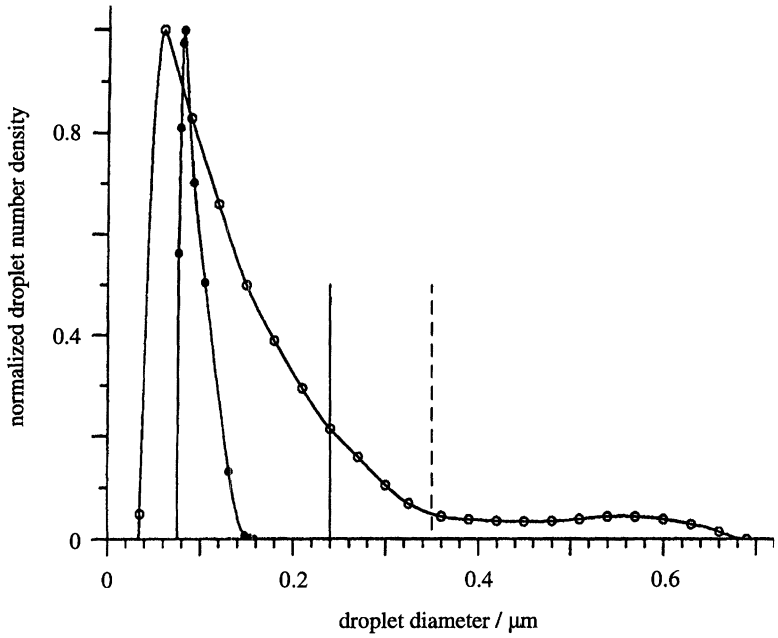

Figure 1. Typical droplet size distributions in a supersonic condensing steam nozzle (computed) and in the exhaust of a low pressure, electricity generating steam turbine (inferred from optical transmission data). ●, nozzle; ○, turbine; – – – Sauter mean; —— mass mean. (Turbine measurements courtesy of P. T. Walters, National Power Technology and Environmental Centre, Leatherhead, U.K.)

droplets in the flow, and no theory currently exists which gives even remote agreement with the available experimental measurements in turbines.

Our inability to understand the nucleation process in steam turbines is surprising, given the success with which condensation in laboratory nozzles can be predicted using a synthesis of the classical theories of homogeneous nucleation and droplet growth with the conservation equations of gas dynamics. Such calculations have now been refined to the extent that the theory, amended by only a modicum of empiricism, gives acceptable agreement with most experiments reported in the literature. (A comparison of calculation with experimental measurements in steady, subcritical condensing flows is described by Young (1982) and an analysis of steady, and periodically unsteady, supercritical flows by Guha & Young (1991).) Recent work by White (1992) also shows good agreement between theory and measurement in the strongly two-dimensional flow field of a stationary cascade of steam turbine blades.

As shown in figure 1, calculations of droplet size spectra in condensing steam nozzles usually indicate a narrow distribution with a comparatively small mean droplet diameter, strongly dependent on the local expansion rate near the Wilson point. Because of the narrowness of the distribution, optical experimental techniques based on measuring the attenuation of light of different wavelengths (Walters 1973) are unable to resolve the details of the spectrum, but register results consistent with a near monodispersed droplet population. In turbines, however, experimental determinations of droplet size spectra give quite different results, the optical characteristics of the medium invariably indicating a broad, strongly skewed, distribution with a much larger mean diameter, typically 0.2–0.6 μm. Quite often,

the distribution is bimodal with a significant proportion of the total mass of liquid contained in a secondary population of droplets having diameters 0.4–1.0 μm (Walters 1988). A typical distribution, inferred from optical measurements in a low pressure steam turbine used for electricity generation, is also shown in figure 1.

Early attempts to describe the phase-transition process in steam turbines followed the work of Gyarmathy (1962) who modelled the turbine by a series of one-dimensional nozzles. Reversion to equilibrium from the supersaturated vapour state was predicted to occur at a well defined Wilson point in a particular blade passage giving rise to a nearly monodispersed population of usually rather small droplets. The nucleation zone was thought to extend over a very short distance in the flow direction, and calculations indicated that the mean droplet size should be very sensitive to turbine inlet conditions, small changes of which had the potential for displacing the Wilson point to new locations of quite different expansion rate. Later calculations of nucleation and droplet growth in two-dimensional turbine cascades (Bakhtar & Alubaidy 1984; Young 1992) displayed characteristics essentially similar to those found in one-dimensional condensation studies, albeit in more complicated and realistic fluid flowfields.

As noted, optical measurements of wetness fraction and droplet spectra in turbines tell quite a different story. The measured spectrum is always broader, and the mean diameter usually larger, than conventional calculations indicate. Furthermore, the spectrum is comparatively insensitive to small changes in turbine inlet conditions, measurements taken on the same machine over a period of years showing excellent reproducibility. Finally, it appears that the reversion process does not occur in very narrow condensation zones, as observed in laboratory nozzles, but generally occupies much greater distances in the flow direction. This behaviour can be deduced from optical measurements which show that the wetness fractions at certain locations in some turbines are considerably lower than the local equilibrium values (Skillings *et al.* 1988).

It is therefore evident that the nucleation of water droplets in turbines involves phenomena which are not reproduced by laboratory experiments on nozzles and stationary cascades but, nevertheless, play a dominating role in the process of phase transition in real machines. Possible explanations include nucleation in blade-wake vortices (Filippov *et al.* 1970), the effects of impurities in the steam (Steltz *et al.* 1983) and the effects of blade-row interaction unsteadiness (Gyarmathy & Spengler 1974). In this paper, consideration is given to the third of these possibilities, namely the effect of the unsteadiness due to the interaction of blade wakes with downstream blade rows. It will be shown that a direct result of these interactions is to dramatically broaden the droplet size distribution giving a general shape and mean diameter much more in keeping with experimental measurements in real turbines. The new theory also predicts that the formation of the liquid phase takes place in a randomly unsteady manner and may encompass a region comprising one or more complete turbine stages in a multistage machine. These results present a radically different perspective of nucleation in turbines from the generally accepted view and, if correct, will have a major influence on the future development of calculation procedures for non-equilibrium steam flow in turbines.

PHILOSOPHICAL TRANSACTIONS OF THE ROYAL SOCIETY A MATHEMATICAL, PHYSICAL & ENGINEERING SCIENCES

2. Temperature fluctuations in multistage turbines

A theory of temperature fluctuations in multistage turbines due to wake–blade interactions was developed by Gyarmathy & Spengler (1974) and forms the starting point for this work. Their primary goal was to offer a physical explanation for the large-scale fluctuations in temperature measured by Wood (1973) in a multistage turbine. These measurements showed that the fluctuation of total temperature at the turbine outlet was comparable with the temperature drop in a blade row. Conventional turbulence alone could not be responsible for fluctuations of such large magnitude.

Gyarmathy & Spengler were concerned with predicting temperature fluctuations in single-phase gas flows but the implications for phase change of a condensing vapour did not escape their attention. The fundamental premise of their theory was that, in passing through a multistage turbine, different fluid particles undergo different fluid mechanical experiences depending on the exact details of their passage through the machine and hence arrive at a given axial location with a wide variety of thermodynamic conditions. They also postulated that, downstream of any turbine stage, the pressure of all the fluid particles would be nearly uniform, but their specific entropies (and hence static temperatures) would vary greatly depending on the dissipation experienced by the particular particle. However, although the path taken by a fluid particle was assumed to be random, the time-averaged dissipation of all the particles must agree with the overall loss distribution in the turbine. This was assumed known, either by direct measurement or from empirical loss correlations.

Gyarmathy & Spengler developed their theory using an informal, intuitive approach which tended to obscure the precise nature of the underlying assumptions. (It also appears that computed variations of *static* temperature were compared with experimentally determined fluctuations of *total* temperature measured in a real turbine by Wood (1973).) It is therefore necessary to re-examine the theory of temperature fluctuations in turbines from a more formal standpoint, before introducing the extensions necessary to describe phase change.

For calculations in the moving blade rows of turbomachines, it is convenient to work in a coordinate system rotating at the turbine angular velocity $\boldsymbol{\Omega}$. In this frame of reference, the conservation equations of mass, momentum and energy for laminar flow can be written

$$(\mathrm{d}\rho/\mathrm{d}t)+\rho\nabla\cdot\boldsymbol{w}=0, \tag{1}$$

$$\rho[(\mathrm{d}\boldsymbol{w}/\mathrm{d}t)+2(\boldsymbol{\Omega}\wedge\boldsymbol{w})+\boldsymbol{\Omega}\wedge(\boldsymbol{\Omega}\wedge\boldsymbol{r})]+\nabla p=\nabla\cdot\sigma, \tag{2}$$

$$\rho\,\mathrm{d}/\mathrm{d}t\,[h_0-\tfrac{1}{2}(\boldsymbol{\Omega}\wedge\boldsymbol{r})^2]-(\partial p/\partial t)=\nabla\cdot[(\sigma\cdot\boldsymbol{w})-\boldsymbol{q}], \tag{3}$$

where p is the pressure, ρ is the density, $\boldsymbol{r}$ is the position vector, $\boldsymbol{w}$ is the velocity vector of a fluid particle in the rotating coordinate system, $h_0=h+\frac{1}{2}w^2$ is the *relative* stagnation specific enthalpy, $\boldsymbol{q}$ is the heat flux vector and σ is the viscous part of the stress tensor. $\boldsymbol{q}$ and σ are given by,

$$\left.\begin{aligned}\boldsymbol{q}&=-k\nabla T,\\ \sigma&=\mu(\nabla\boldsymbol{w}+\nabla\boldsymbol{w}^{\mathrm{t}})+\lambda(\nabla\cdot\boldsymbol{w})\,U,\end{aligned}\right\} \tag{4}$$

where k is the thermal conductivity, T is the static temperature, μ is the dynamic viscosity, λ is the second viscosity ($-2\mu/3$ for a monatomic gas) and U is the unit tensor. $\mathrm{d}/\mathrm{d}t=\partial/\partial t+\boldsymbol{w}\cdot\nabla$ is the substantive derivative in the rotating frame of

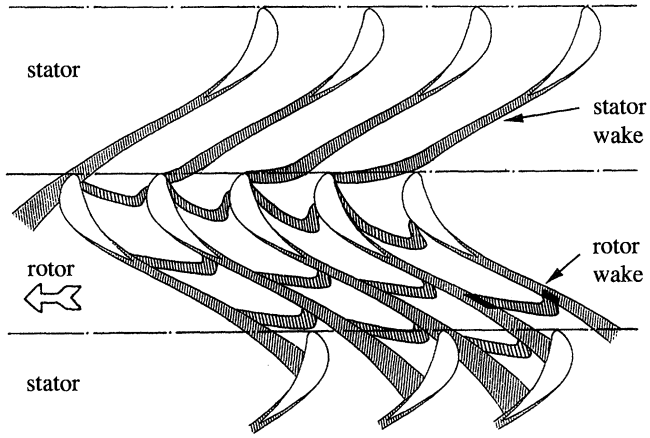

Figure 2. Schematic diagram of the passage of blade wakes through successive blade rows.

reference and $\partial/\partial t$ is the partial derivative at a position fixed relative to the moving coordinate system. The combination of terms

$$I = h_0 - \tfrac{1}{2}(\boldsymbol{\Omega} \wedge \boldsymbol{r})^2, \tag{5}$$

is known as the specific rothalpy. For inviscid, non-conducting steady flow, relative to the rotating blades, the specific rothalpy of a fluid particle remains constant.

For flow in stationary blade rows, the conservation equations are obtained by setting $\boldsymbol{\Omega} = 0$ in (1)–(3). $\mathrm{d}/\mathrm{d}t$ is then the substantive derivative and $\boldsymbol{w}$ the velocity in the stationary coordinate system.

The term $-\nabla\cdot\boldsymbol{q}$ in the energy equation (3) represents the rate at which heat is conducted to a fluid particle of unit volume from its surroundings. $\nabla\cdot(\sigma\cdot\boldsymbol{w})$ represents the rate at which the viscous stresses do work on the same particle. (This term was neglected by Gyarmathy & Spengler.) The expression $(\sigma\cdot\boldsymbol{w})-\boldsymbol{q}$ can be simplified by substituting (4) and the definition of h_0 to give

$$(\sigma\cdot\boldsymbol{w})-\boldsymbol{q} = \mu(\boldsymbol{w}\cdot\nabla)\,\boldsymbol{w} + \mu\nabla(\tfrac{1}{2}w^2) + \lambda(\nabla\cdot\boldsymbol{w})\,\boldsymbol{w} + (k/c_p)\,\nabla(h_0 - \tfrac{1}{2}w^2),$$

where c_p is the isobaric specific heat capacity. Assuming a Prandtl number $(c_p\mu/k)$ of unity (the Prandtl number for low pressure steam is about 0.9) and neglecting viscous normal stresses in the flow direction,

$$(\sigma\cdot\boldsymbol{w})-\boldsymbol{q} \approx (k/c_p)\,\nabla h_0. \tag{6}$$

Hence, (3) can be written

$$\rho\,\mathrm{d}/\mathrm{d}t[h_0 - \tfrac{1}{2}(\boldsymbol{\Omega}\wedge\boldsymbol{r})^2] \approx \frac{\partial p}{\partial t} + \nabla\cdot\left[\frac{k}{c_p}\nabla h_0\right]. \tag{7}$$

Figure 2 is a schematic diagram of the way in which the wakes from one blade row interact with, and are segmented by, the following row. It can be clearly seen that dissipation occurring in successive blade rows can become superposed in certain fluid particles (the darkly shaded areas). The assumption is now made that the fluctuations of static temperature at a given point in a turbine are dominated by the wake–blade interactions in the stages upstream. 'True' turbulent fluctuations in the blade boundary layers, wakes and free stream are ignored in the present theory. This is not meant to suggest that shear-layer turbulence plays no part in the formation of the

liquid phase in steam turbines. (Indeed, the type of wake–condensation effect postulated by Filippov *et al.* (1970) is due entirely to temperature fluctuations caused by eddy shedding from the blade trailing-edges.) However, in a multistage turbine with a substantial number of blade rows, it is postulated that the large-scale fluctuations in static temperature will result mainly from wake–blade interactions and that 'true' turbulence will exert its influence by superimposing a small amplitude, higher frequency 'fuzziness' on the overall fluctuation pattern. Confirmation or otherwise of this hypothesis must await further investigation but it should be clearly understood that unsteadiness due to turbulence is 'averaged out' in this study.

The analysis proceeds by time averaging the conservation equations using the conventional methods introduced by Reynolds and Favre. Thus, the variables appearing in equations (1)–(3) are decomposed into mean and fluctuating components (Kuo 1986, ch. 7),

$$\boldsymbol{w} = \bar{\boldsymbol{w}} + \boldsymbol{w}' = \tilde{\boldsymbol{w}} + \boldsymbol{w}'', \quad p = \bar{p} + p' = \tilde{p} + p'', \quad \text{etc.},$$

where $\bar{\boldsymbol{w}}$ and $\bar{p}$ represent Reynolds-averaged quantities and $\tilde{\boldsymbol{w}}$ and $\tilde{p}$ represent Favre-averaged quantities. After time averaging, the conservation equations take the form

$$(\mathrm{d}\bar{\rho}/\mathrm{d}t) + \bar{\rho}\nabla\cdot\tilde{\boldsymbol{w}} = 0, \tag{8}$$

$$\bar{\rho}[(\mathrm{d}\tilde{\boldsymbol{w}}/\mathrm{d}t) + 2(\boldsymbol{\Omega}\wedge\tilde{\boldsymbol{w}}) + \boldsymbol{\Omega}\wedge(\boldsymbol{\Omega}\wedge\boldsymbol{r})] + \nabla\bar{p} = \nabla\cdot(\bar{\sigma} + \bar{\sigma}_{\mathrm{t}}), \tag{9}$$

$$\bar{\rho}(\mathrm{d}/\mathrm{d}t)[\tilde{h}_0 - \tfrac{1}{2}(\boldsymbol{\Omega}\wedge\boldsymbol{r})^2] - \partial\bar{p}/\partial t = \nabla\cdot(\overline{\sigma\cdot\boldsymbol{w}} - \bar{\boldsymbol{q}}) + \nabla\cdot(\bar{\sigma}_{\mathrm{t}}\cdot\tilde{\boldsymbol{w}} - \bar{\boldsymbol{q}}_{\mathrm{t}}), \tag{10}$$

where $\bar{\sigma}_{\mathrm{t}}$ is the Reynolds stress tensor and $\bar{\boldsymbol{q}}_{\mathrm{t}}$ is the turbulent energy flux vector defined by

$$\bar{\sigma}_{\mathrm{t}} = -\overline{\rho\boldsymbol{w}''\boldsymbol{w}''}, \quad \bar{\boldsymbol{q}}_{\mathrm{t}} = \overline{\rho\boldsymbol{w}''(h'' + \tfrac{1}{2}w''^2)}. \tag{11}$$

The combination of terms,

$$\tilde{I} = \tilde{h}_0 - \tfrac{1}{2}(\boldsymbol{\Omega}\wedge\boldsymbol{r})^2, \tag{12}$$

is the Favre-averaged specific rothalpy. $\mathrm{d}/\mathrm{d}t = (\partial/\partial t) + \tilde{\boldsymbol{w}}\cdot\nabla$ is the substantive derivative following an (imaginary) mean-property fluid particle along a mean pathline defined by the field lines of the Favre-averaged velocity vector field $\tilde{\boldsymbol{w}}$. All future references in this paper to 'fluid particles' and their 'pathlines' imply this meaning.

An integral, time-averaged form of the energy equation can be obtained without approximation by integrating (10) over a control volume comprising a complete blade row and over a time period corresponding to the passing of one blade passage. The result (true for stationary or moving blade rows) is that, irrespective of the effects of viscosity and turbulence, the mass-flow-weighted, time-averaged value of specific rothalpy ($\tilde{I}_\infty$) remains constant between the blade inlet and outlet planes. (The precise conditions for this to be true (Lyman 1992) are: (i) zero velocity slip at the blade surfaces; (ii) all solid surfaces adiabatic; and (iii) neglect of the effect of the casing or hub moving relative to the blades.)

Equation (10) shows, however, that the specific rothalpy of individual fluid particles may well be influenced by molecular viscosity, heat conduction and turbulent transport effects. Furthermore, simplification of the time-averaged energy equation is seriously hampered by the lack of a suitably general turbulence model. However, if it is agreed (i) to neglect the Reynolds normal stresses in the flow direction; (ii) to represent the Reynolds shear stresses and turbulent heat fluxes by

simple eddy–viscosity and eddy–conductivity models; and (iii) to assume a turbulent Prandtl number of unity, then by a similar analysis to that leading to equation (6)),

$$\bar{\sigma}_t \cdot \tilde{\boldsymbol{w}} - \bar{\boldsymbol{q}}_t \approx (k_t/c_p)\nabla \bar{h}_0 \approx \mu_t \nabla \bar{h}_0, \tag{13}$$

where k_t and μ_t are the turbulent heat conductivity and viscosity respectively. A good approximation to the time-averaged energy equation, reflecting the correct physical behaviour, is thus,

$$\bar{\rho}\, \mathrm{d}/\mathrm{d}t[\tilde{h}_0 - \tfrac{1}{2}(\boldsymbol{\Omega} \wedge \boldsymbol{r})^2] \approx \partial \bar{p}/\partial t + \nabla \cdot \left[\frac{k + k_t}{c_p} \nabla \bar{h}_0\right]. \tag{14}$$

Equation (14) shows that the specific rothalpy of a fluid particle is affected by pressure fields which are unsteady relative to the blades. Such pressure fields are associated with the potential–flow interactions of the upstream and downstream blade rows and also with the passage of wakes generated upstream. Without undertaking a major computational exercise (i.e. the numerical simulation of the unsteady blade-row interactions) it is difficult to assess the magnitude of these effects, and so it is here assumed that all pressure fields are steady with respect to both stationary and rotating blades (i.e. $\partial \bar{p}/\partial t = 0$ everywhere). This assumption (which also implies that, between blade rows, the pressure is spatially uniform in the circumferential direction) is realistic when the axial spacing between blade rows is large, but becomes more questionable as the axial gap is reduced.

Equation (14) also shows that the specific rothalpy of individual fluid particles is affected by diffusive processes which tend to eradicate gradients of relative stagnation specific enthalpy. Given sufficient time, therefore, the specific rothalpy of all fluid particles would ultimately attain the mass-flow-weighted, time-averaged value $\tilde{I}_\infty$. Were the 'equalization time' less than the time required for a fluid particle to pass through a blade row, no temperature fluctuations due to wake–blade interactions would be observed. On the other hand, were the equalization process very slow, the second term on the right-hand side of (14) would be zero and the rothalpy of each fluid particle would remain constant.

Gyarmathy & Spengler (1974) also considered the eradication of non-uniformities by molecular and turbulent energy transfer but they viewed the process simply in terms of the equalization of *static* enthalpy (or temperature) gradients. However, apart from details such as these, the problem still remains of estimating the rate at which the diffusive process proceeds and to do this successfully requires detailed knowledge (which is not available) of the magnitude and variation of the turbulent heat conductivity k_t. The analysis presented by Gyarmathy & Spengler led them to conclude that very little mixing out would occur during the passage of a wake through a blade row. However, this conclusion was based on the assumption that the magnitude of the ratio k_t/k (or μ_t/μ) was less than five and actual values are probably very much higher. An approximate analysis of wake diffusion in the appendix below suggests that relative stagnation enthalpy variations in wakes are typically eroded by 20–30% per blade row.

An exact representation of the final term in (14) is clearly out of the question but, nonetheless, it is important to estimate the variation of fluid particle rothalpy due to molecular and turbulent diffusion. Equation (14) is therefore replaced by the model equation

$$\mathrm{d}I/\mathrm{d}t = -(I - I_\infty)/\tau_E, \tag{15}$$

where τ_E is a time constant quantifying the rate at which stagnation enthalpy

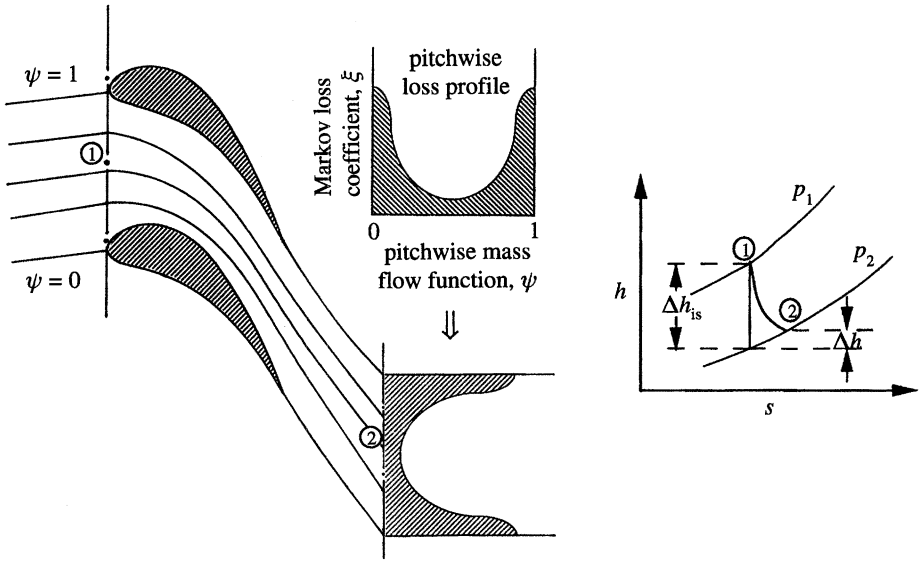

Figure 3. Specification of the pitchwise loss profile for a blade row.

gradients are eroded (the tildes having been dropped for convenience). $\tau_E = 0$ implies instantaneous, and $\tau_E \to \infty$ implies infinitely slow, equilibration. The highly simplified analysis of wake diffusion in the appendix suggests the expression

$$\tau_E \approx \left(\frac{\delta}{\pi L}\right)^2 \frac{Re}{1+(\mu_t/\mu)} \Delta t, \tag{16}$$

where $Re = \rho \bar{V}_x L/\mu$ is the Reynolds number based on the mean axial velocity $\bar{V}_x$ and axial cord length L, δ is the width of the wake and Δt is the time for a fluid particle to pass through the blade row. However, given the difficulty of accurate representation, it may be preferable to treat τ_E as an empirical constant. Equation (15) can then be integrated to give

$$(I - I_\infty) = (I_1 - I_\infty) \exp(-t/\tau_E), \tag{17}$$

where t is the time measured along a fluid particle pathline and I_1 is the rothalpy at blade inlet.

The thermodynamic state and velocity of a fluid particle are fully defined by its static pressure, specific rothalpy, flow direction and specific entropy. Downstream of a blade row, the static pressure and flow direction for all fluid particles are assumed to be the circumferential- and time-averaged values and the specific rothalpy is given by (17). It remains to estimate the entropy increase of the particle in passing through the blade passage, a quantity which evidently depends on the pathline taken by the particle. Thus, fluid particles that by chance travel near the centre of the passage expand almost isentropically, whereas those that enter the blade boundary layers experience maximum loss. For each blade row in the turbine, it is therefore necessary to establish a detailed loss model (experimental or empirical) from which the entropy increase (or decrease) of individual fluid particles can be estimated.

The method by which this is done is similar to that described by Gyarmathy & Spengler (1974). As shown in figure 3, a 'loss profile' is constructed to represent the pitchwise distribution (from the suction to the pressure surface) of the loss in the

blade row. For the calculations described below, the loss profiles were established at the inlet plane of the downstream blade row, but other, more detailed, and perhaps more accurate, methods of specifying the distribution of losses in a blade passage can be envisaged. The loss profile is a curve of the local Markov loss coefficient ξ (defined in equation (18) below) against the dimensionless mass flowrate ψ (which runs from zero at the suction surface streamline to unity at the pressure surface streamline). With reference to figure 3,

$$\xi = 2\Delta h/w_2^2. \tag{18}$$

The area under the profile represents the mass-flow-weighted average loss coefficient. When computing phase change, the streamwise, as well as the pitchwise, distribution of loss may be important and it is more convenient to represent the loss in terms of a polytropic efficiency of expansion η. For the results presented below, a constant value of η was used but more complex variations could be introduced if desired. (It should be noted that Guha (1990) has shown that the resulting droplet spectrum is comparatively insensitive to the streamwise distribution of loss.) The polytropic efficiency is related to the Markov loss coefficient by

$$\eta \int_1^2 \frac{\mathrm{d}p}{\rho} = \Delta h_{\mathrm{is}} - \tfrac{1}{2}\xi w_2^2. \tag{19}$$

The pitchwise loss profiles represent the time-averaged entropy increase along particular pathlines but individual fluid particles associated with the passage of wakes may exit from the blade row at different conditions because, on entry, their static temperatures and velocities deviate from the mean. Owing to the diffusive action of viscosity, heat conduction and turbulent transport effects, however, there will be a general tendency for the static enthalpy and velocity of a particle to equilibrate to the downstream mean values of that particular pathline. Furthermore, because the laminar and turbulent Prandtl numbers are both close to unity, the Reynolds analogy suggests that the eradication of velocity and temperature gradients proceeds at about the same rate.

Taking the scalar product of $\boldsymbol{w}$ with the momentum equation (9) and subtracting from the energy equation (10) gives the thermodynamic form, which can be written

$$\rho T \frac{\mathrm{d}s_{\mathrm{A}}}{\mathrm{d}t} = \rho \frac{\mathrm{d}h}{\mathrm{d}t} - \frac{\mathrm{d}p}{\mathrm{d}t} = \nabla \cdot \left(\frac{k + k_{\mathrm{t}}}{c_p} \nabla h \right) + \rho \Phi, \tag{20}$$

where $\mathrm{d}s_{\mathrm{A}}/\mathrm{d}t$ is the rate of increase of fluid particle specific entropy and Φ is the 'dissipation function'. Modelling of the right-hand side of (20) for a general fluid particle is very difficult and an approximate representation is all that is feasible. Accordingly, it is assumed that the dissipation is similar to the time-mean case in the sense that it can be represented by the same polytropic efficiency η (which varies from streamline to streamline). The divergence of the heat flux is modelled in a similar way to the diffusive term in equation (14). Hence,

$$T \frac{\mathrm{d}s_{\mathrm{A}}}{\mathrm{d}t} = \frac{\mathrm{d}h}{\mathrm{d}t} - \frac{1}{\rho}\frac{\mathrm{d}p}{\mathrm{d}t} = -\frac{(1-\eta)}{\rho}\frac{\mathrm{d}p}{\mathrm{d}t} - \frac{(h - h_\infty)}{\tau_{\mathrm{E}}}, \tag{21}$$

where τ_{E} is the same time constant as in equation (15) and the definition of h_∞ is best appreciated by reference to figure 4. For $\tau_{\mathrm{E}} = 0$, equilibration of static temperature is instantaneous, $h = h_\infty$ at all times, and the fluid particle expands along the time-mean condition line. For $\tau_{\mathrm{E}} \to \infty$, equilibration is infinitely slow.

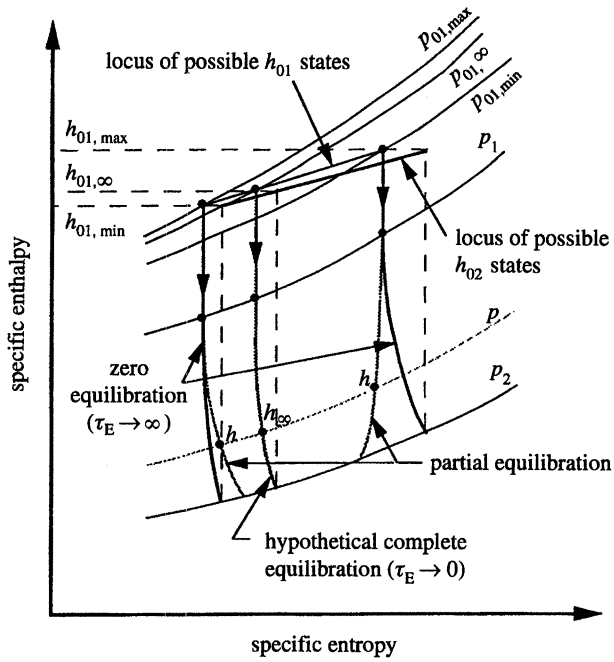

Figure 4. Variation of state for a fluid particle passing through a blade row.

The magnitude of the static temperature fluctuations at any position in a multistage turbine can now be obtained by the following sequence of calculations:

(i) The static pressure distribution throughout the turbine is established by a suitable steady-flow calculation (e.g. a streamline-curvature throughflow procedure).

(ii) Loss profiles are constructed for each blade row from experimental or empirical loss coefficient data and the value of the equilibration time-constant τ_E is specified.

(iii) A fluid particle is 'launched' at the turbine inlet with the given inlet stagnation pressure and temperature. A random number between zero and unity is generated to fix the pitchwise position (i.e. the value of ψ) of the particle pathline through the first blade row. The corresponding value of ξ (and hence η) is obtained from the relevant loss profile and the static enthalpy of the particle at exit can then be calculated from (21). For the first blade row, $I_\infty = I_1$ for all particles, and this defines the exit velocity.

(iv) Construction of the velocity triangle at blade exit establishes the relative inlet velocity to the next blade row and the corresponding value of the new specific rothalpy. Assuming the pitchwise position of the particle pathline through the second blade row to be completely independent of the path through the first, another random number between zero and unity is generated to obtain a new value of ψ. The exit static enthalpy h_2 and relative velocity $\boldsymbol{w}_2$ are then calculated from equations (15) and (21), this time using the loss profile for the second blade row.

(v) Similar calculations are repeated for each blade row of the turbine in turn. Values of the particle static temperature at all points of interest are stored for future use.

(vi) The procedure of (iii)–(v) is repeated for a large number of fluid particles. After each sequence of calculations, the mean static temperature, the standard

deviation and any other statistical properties required are computed at all points of interest. The launch of fluid particles continues until the statistical properties remain constant within a previously specified convergence criterion. For a six-stage low-pressure turbine, this may require the calculation of some 10^4 fluid particle histories.

The assumption that the particle path through one blade row is completely independent of its passage through the previous row is not correct. As shown by Kerrebrock & Mikolajczak (1970), there is a tendency in turbines for the wakes from one blade row to migrate towards the suction surfaces of the blades in the next. A fluid particle entrained in one boundary layer therefore has a higher probability than other particles of being entrained in the boundary layers of succeeding blade rows. This effect could be modelled by weighting the selection of ψ with a factor dependent on the previous history of the particle. However, such sophistication has not been introduced in the present calculations.

3. The formation and growth of the liquid phase

The statistical analysis of the previous section can be extended to investigate the effect of wake–blade interactions on the formation of the liquid phase in turbines (Bakhtar & Heaton 1988). The major assumption in extending the theory is that the classical theories of homogeneous nucleation and droplet growth realistically describe the process of phase change for *individual* fluid particles. In other words, if the pressure–time and temperature–time variations of a fluid particle during its passage through the turbine can be accurately specified, then it is assumed that the theories of nucleation and droplet growth correctly describe the rate of formation of the liquid phase within that particle. For different fluid particles, phase change will be initiated at different locations in the machine, depending on the dissipation suffered by the particle. This is in contrast to the usual model of nucleation in turbines which assumes phase change to be governed by the time-averaged fluid properties and to occur at a single, well-defined location. (It should be noted that the theory only considers liquid formation by homogeneous nucleation. The possibility of nucleation on foreign particles is excluded.)

The physical processes leading to the formation and growth of liquid droplets have been described in many publications (see, for example, Young 1982). Briefly, when a fluid particle is 'launched' at the turbine inlet, it is initially composed of superheated vapour. During its passage through the machine, its pressure and temperature fall and at some point its thermodynamic state is dry saturated. In the rapid expansion which follows, there is insufficient time for nucleation to occur and the vapour remains dry but becomes 'subcooled' because its temperature T_v is lower than the local saturation temperature T_s. Departures from equilibrium of the metastable vapour are measured by the subcooling ΔT, defined by

$$\Delta T = T_s - T_v. \tag{22}$$

As the subcooling rises, the rate of nucleation of liquid droplets increases dramatically. Condensational growth on these droplets then liberates 'latent heat' which is conducted back to the vapour, ultimately causing the subcooling to fall and nucleation to cease. The point of maximum subcooling is termed the Wilson point. Downstream of the Wilson point the subcooling decreases almost exponentially as a result of very rapid droplet growth and the steam reaches near equilibrium (i.e. $\Delta T \to 0$). The subsequent expansion of the vapour–droplet mixture, comprising the

PHILOSOPHICAL TRANSACTIONS OF THE ROYAL SOCIETY A MATHEMATICAL, PHYSICAL & ENGINEERING SCIENCES

fluid particle, involves departures from thermal equilibrium (because droplet growth itself is a rate process which may not be sufficiently rapid to maintain the local equilibrium), but generally, the droplet number per unit mass remains constant. It is only in regions of very high expansion rate where further nucleation of additional droplets becomes significant.

Following nucleation, each fluid particle contains a large number of droplets of different sizes. The continuous distribution of droplet radii is discretized into a number of droplet groups such that group i contains n_i droplets per unit mass of mixture, each of radius r_i, density ρ_i and mass $m_i = 4\pi r_i^3 \rho_i/3$. The wetness fraction y is thus given by

$$y = \Sigma y_i = \Sigma n_i m_i = \Sigma 4\pi r_i^3 \rho_i n_i/3, \tag{23}$$

where the summation is over all the droplet groups. Neglecting the volume occupied by the droplets, the mixture density ρ is given by

$$\rho = \rho_v/(1-y), \tag{24}$$

where ρ_v is the density of the vapour phase. The mixture specific enthalpy h is

$$h = (1-y)\, h_v + \Sigma y_i h_i, \tag{25}$$

where h_v is the vapour specific enthalpy and h_i is the specific enthalpy of a group i droplet. (Note that ρ_v and h_v must be evaluated at the local vapour pressure p and temperature T_v which generally corresponds to a subcooled state. Similarly, the wetness fraction y does not necessarily correspond to the local equilibrium value and must be determined through a non-equilibrium calculation procedure.)

It is assumed that the velocity slip between droplets and vapour is negligible. This approximation is satisfied well for the tiny (submicron) 'fog' droplets in turbines and implies that, once nucleated, the same droplets reside in a given fluid particle throughout its passage through the machine. The important mathematical consequence of this assumption is (Young 1984) that the conservation equations for the multiphase flow of the vapour–droplet mixture are identical to their single-phase counterparts (i.e. equations (8)–(10)) so long as the density ρ and the specific enthalpy h are taken to be the non-equilibrium mixture values defined by (24) and (25).

Equation (21) also applies to non-equilibrium condensing flows but it is important to appreciate that $\mathrm{d}s_A/\mathrm{d}t$ represents the rate of increase of fluid particle specific entropy due solely to the 'aerodynamic' effects of viscosity, heat conduction and turbulence. Entropy production due to interphase heat and mass transfer is implicitly included in the other terms. Introducing equation (25), equation (21) can be written

$$(1-y)\frac{\mathrm{d}h_v}{\mathrm{d}t} + \Sigma y_i \frac{\mathrm{d}h_i}{\mathrm{d}t} - \Sigma (h_v - h_i)\frac{\mathrm{d}y_i}{\mathrm{d}t} = \frac{\eta}{\rho}\frac{\mathrm{d}p}{\mathrm{d}t} - \frac{(h-h_\infty)}{\tau_E}. \tag{26}$$

Equation (26) is complemented by expressions for the $\mathrm{d}y_i/\mathrm{d}t$. The derivation of these droplet growth equations can be found in Young & Guha (1991) but the essential result is

$$(h_v - h_i)\frac{\mathrm{d}y_i}{\mathrm{d}t} - y_i \frac{\mathrm{d}h_i}{\mathrm{d}t} = \frac{(1-y)\, c_{pv}(\Delta T - \Delta T_{\mathrm{cap},i})}{\tau_{Ti}}, \tag{27}$$

where τ_{Ti} has the dimension of time and is a function of r_i, n_i and the local vapour conditions. The droplet number density n_i is obtained from the nucleation equation (Guha & Young 1991). $\Delta T_{\mathrm{cap},i}$ is the capillary subcooling of the droplets

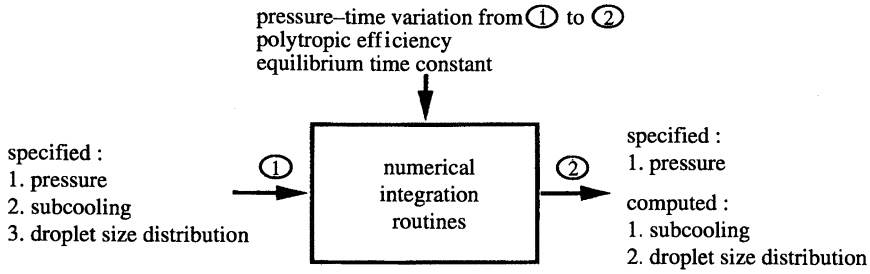

Figure 5. 'Black-box' for computing the thermodynamics of phase change.

($\Delta T_{\mathrm{cap},i} = T_{\mathrm{s}} - T_i$) and is given by the well-known Kelvin–Helmholtz equation. It is negligible for established droplets but is very significant for fresh nuclei. One growth equation of the form (27) is required for each droplet group present.

The vapour subcooling ΔT is now introduced into (26). Assuming the vapour to behave as a perfect gas with specific gas constant R_{v} and isobaric specific heat capacity c_{pv}, and using (27) and the Clausius–Clapeyron equation,

$$\frac{\mathrm{d}p}{p} = \frac{h_{\mathrm{fg}}}{R_{\mathrm{v}} T_{\mathrm{s}}} \frac{\mathrm{d}T_{\mathrm{s}}}{T_{\mathrm{s}}} \tag{28}$$

(where h_{fg} is the specific enthalpy of evaporation), gives

$$\frac{\mathrm{d}(\Delta T)}{\mathrm{d}t} = -\frac{(\Delta T - \Delta T_{\mathrm{cap}})}{\tau_{\mathrm{T}}} - \left(1 - \frac{c_{pv} T_{\mathrm{s}}}{h_{\mathrm{fg}}} \frac{T_{\mathrm{s}}}{T_{\mathrm{v}}}\right)\left(\frac{R_{\mathrm{v}} T_{\mathrm{v}}}{c_{pv}}\right)\dot{p} + \left[(1-\eta)\frac{R_{\mathrm{v}} T_{\mathrm{v}}}{c_{pv}}\dot{p} + \frac{(h - h_{\infty})}{(1-y)\, c_{pv}\, \tau_{\mathrm{E}}}\right]. \tag{29}$$

τ_{T} represents the overall thermal relaxation time of the mixture and is related to the contribution from individual group i droplets via the summation

$$1/\tau_{\mathrm{T}} = \Sigma\, 1/\tau_{\mathrm{T}i}. \tag{30}$$

Similarly,

$$\Delta T_{\mathrm{cap}} = \Sigma\, (\tau_{\mathrm{T}}/\tau_{\mathrm{T}i})\, \Delta T_{\mathrm{cap},i}. \tag{31}$$

Outside the nucleation zone, ΔT_{cap} is usually negligible. $\dot{p}$ is defined by $\dot{p} = \mathrm{d}(\log_{\mathrm{e}} p)/\mathrm{d}t$ and in a turbine is generally a *negative* quantity ($-\dot{p}$ being termed the rate of expansion). Equation (29) shows that the growth or decay of the vapour subcooling of an individual fluid particle is controlled by three distinct processes. The first term on the right-hand side represents the natural tendency of the mixture to relax to equilibrium in the absence of other 'driving forces'. The second term describes the response to the local expansion rate and is usually the dominating term in regions where $-\dot{p}$ is high. The third term represents the dissipation due to aerodynamic effects and heat transfer (between the fluid particle and its surroundings).

Equations (27) and (29) describe completely the formation and growth of liquid-phase droplets in a fluid particle if the pressure–time variations, $\mathrm{d}p/\mathrm{d}t$, the polytropic efficiency, η, and the equilibration time-constant, τ_{E}, are all specified. In this respect, the thermodynamic aspects of phase change can be completely divorced from fluid-dynamical considerations so that it is possible to construct an integration procedure for (27) and (29) which is effectively independent of any particular computational fluid dynamics application. Such a procedure is illustrated in figure 5. The 'black box' contains computational routines for the numerical integration of the equations. The input is the full steam condition at state 1 (pressure, subcooling and

droplet size distribution), together with the pressure–time variation of the fluid particle between states 1 and 2, the polytropic efficiency η and the time constant τ_E. The output is the full steam condition at state 2. The only interaction with the fluid dynamics of the problem is in the specification of η, τ_E and the pressure–time variation.

The development of the computational routines within the black box represents a comparatively major undertaking and has been fully described by Guha & Young (1991) and Young (1992) in other contexts. The routines are sufficiently general and robust to deal with any type of nucleating or wet steam flow and (in contrast to many procedures reported in the literature) full details of the droplet spectrum following nucleation are retained in the calculations. Successive nucleations after the primary are dealt with as a matter of course should the expansion be sufficiently rapid to generate the high levels of subcooling required.

The calculation of phase change in steam turbines follows a similar pattern to the calculation of temperature fluctuations in single-phase flow described previously. Fluid particles are launched from the turbine inlet (where the steam is superheated) and their progress through successive blade rows is specified by the generation of random numbers to define the particle pathlines. After crossing the saturation line, however, the calculations are very much more complicated and time consuming than their single-phase counterparts because it is necessary to enter the black box routines to compute the growth of existing droplets and the nucleation of fresh groups.

An important difference between single-phase and condensing-flow calculations is in the specification of the pressure variation for a fluid particle. In the Gyarmathy & Spengler scheme, it was only necessary to specify the pressure at computing stations between the blade rows. However, the dynamics of phase change are intimately related to the local expansion rate and, for condensing-flow calculations, it is necessary to supply a detailed pressure–time history for each fluid particle passing through each blade row. For the results presented below, a single (circumferentially averaged) pressure–time variation based on an axisymmetric streamline-curvature throughflow solution was adopted for all fluid particles. It is possible, however, that blade-to-blade variations in pressure distribution exert a strong influence on the liquid-phase formation (Young 1992). Currently, work is in progress in devising methods for representing these variations sufficiently accurately but without the necessity for performing expensive cascade-plane calculations for each blade row.

For each fluid particle, the subcooling and droplet size distribution at all points of interest are recorded. The time-mean wetness fraction and other statistical properties can then be computed to obtain a quantitative picture of the process of phase change and liquid growth throughout the machine. In a six-stage low pressure turbine, some 10^4 fluid particle calculations must be undertaken on each streamsurface to obtain converged statistical properties and, hence, the procedure is comparatively expensive in terms of CPU (Central Processing Unit) time.

4. Theoretical predictions of phase change in turbines

To investigate the effects of temperature fluctuations due to wake segmentation on the condensation process, the flow through the low pressure stages of a 320 MW turbine was analysed. The turbine was manufactured by the Italian company Ansaldo and the complete geometry is available in the literature (AGARD 1981). The

PHILOSOPHICAL TRANSACTIONS OF THE ROYAL SOCIETY A MATHEMATICAL, PHYSICAL & ENGINEERING SCIENCES

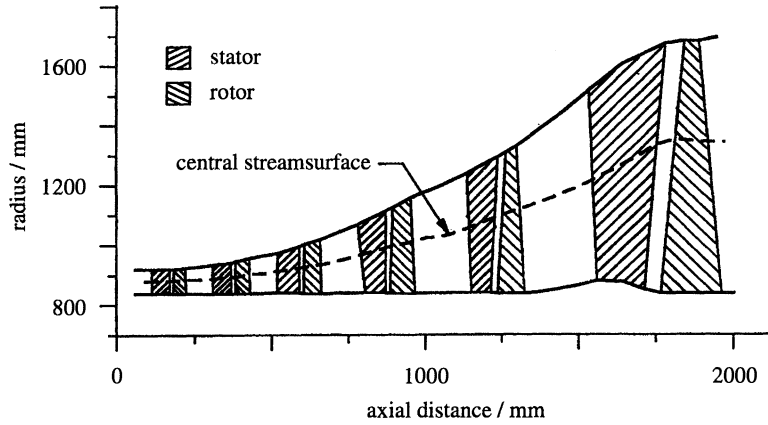

Figure 6. Meridional cross-section of the six-stage, low pressure cylinder of the Ansaldo 320 MW turbine showing the streamsurfaces computed by the axisymmetric throughflow procedure.

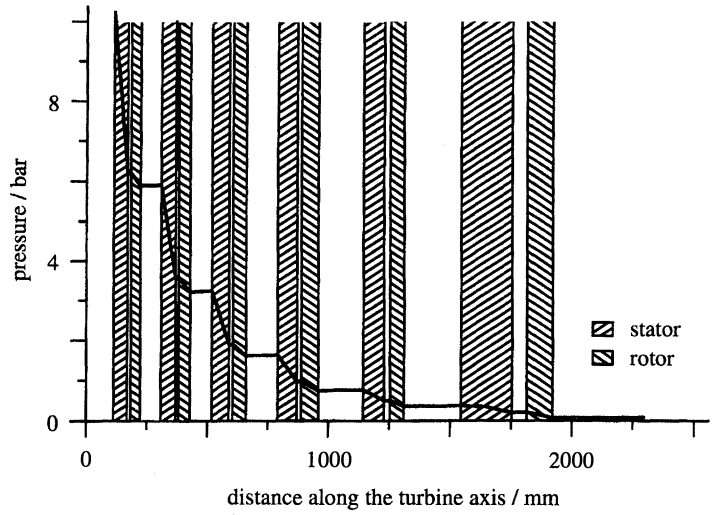

Figure 7. Throughflow prediction of the axial variation of pressure in the low pressure cylinder of the Ansaldo turbine.

low pressure section has six stages and the cross-section in the meridional plane is shown in figure 6. Each stage consists of a stator followed by a rotor and hence there are twelve blade rows altogether in the turbine.

The circumferentially averaged pressure variation through the turbine was calculated using the streamline curvature throughflow method of Denton (1978). A total of nine streamsurfaces and 38 quasi-orthogonals were used for solving the equations of motion in the meridional plane. The converged solution generated time-mean, circumferentially averaged, flow properties, such as pressure and velocity, at each node point formed by the intersection of a streamsurface and a quasi-orthogonal. However, the analysis of nucleation is confined to the central streamsurface which is located near the mid-span of the blades as shown in figure 6. The calculated pressure variation on this central streamsurface as a function of the axial distance through the machine is shown in figure 7. Being a reaction turbine, the pressure decreases continuously within each blade row but remains almost constant

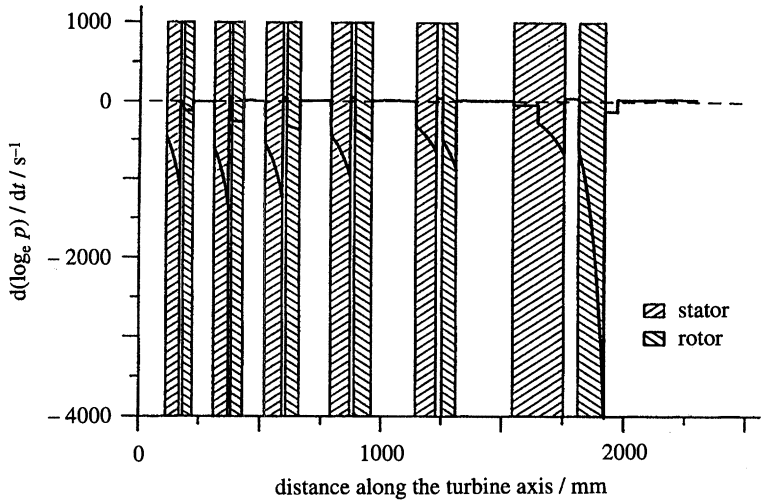

Figure 8. Axial variation of the rate of expansion ($-\dot{p}$) in the Ansaldo turbine.

in the inter-blade and interstage gaps. A corollary of neglecting any fluctuation or circumferential variation in pressure is that all fluid particles moving on the same streamsurface experience the same pressure field.

Because homogeneous nucleation is a rate process, it is strongly dependent on the rate of change of pressure (i.e. $\dot{p} = \mathrm{d}(\log_e p)/\mathrm{d}t$) rather than its absolute level. The variation of $\dot{p}$ through the turbine can easily be calculated from figure 7 because the axial velocity variation is also known from the throughflow calculation. The variation of $\dot{p}$ is plotted in figure 8 and it can be seen that the rate of expansion consistently increases within each blade row and attains very high values in the final stage rotor passage. Between blade rows the expansion rate is almost zero because the pressure remains almost constant.

The advantage of separating the thermodynamical calculations from the fluid mechanics is now apparent. Given the variation of $\dot{p}$ as input, the black box of figure 5 becomes a self-contained computational module capable of predicting the thermodynamic states of any fluid particle passing through the turbine. The only remaining task is to specify the loss profiles downstream of each blade row. For lack of experimental data, a parabolic pitchwise variation of loss was assumed such that the total loss (i.e. the area under the loss profile) was 8% of the isentropic enthalpy drop in each blade row. (This figure was obtained from empirical loss correlations and is unlikely to be seriously in error.) The maximum loss coefficient at each control plane was then 24% at the blade surfaces ($\psi = 0$ or 1) and the minimum value was zero at mid-pitch ($\psi = 0.5$). The implications of these assumptions are discussed later.

The physical characteristics are best explained by adopting a Lagrangian viewpoint of a fluid particle as it passes through the turbine. As described in the previous sections, different fluid particles experience different amounts of dissipation and heat transfer, depending on the particular pathline followed. Two limiting cases can be identified and are discussed in detail below. At one extreme are the fluid particles which always follow the mid-pitch pathline in each blade row and consequently suffer no dissipation. They pursue an isentropic path to the Wilson point. At the other extreme are those particles which negotiate the regions of maximum loss in

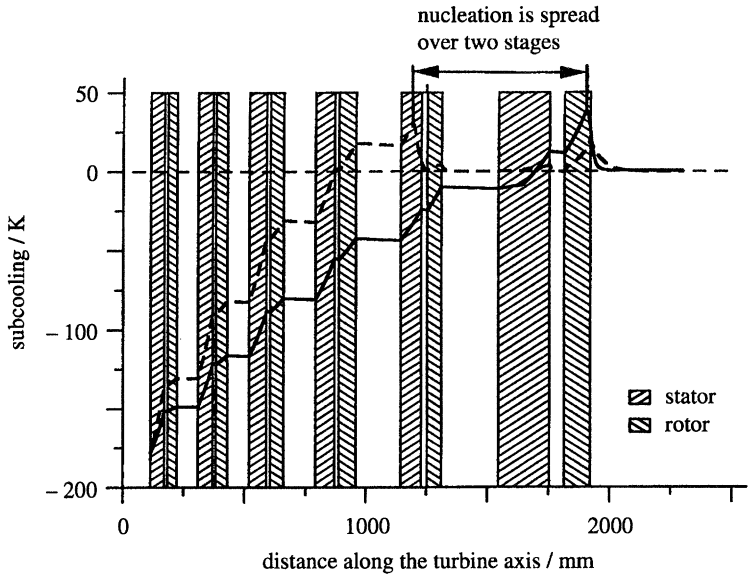

Figure 9. Axial variation in the Ansaldo turbine of vapour subcooling for two fluid particles representing the extreme cases of zero dissipation (– – –) and maximum dissipation (——).

each blade-row (24 % in the present example). Other fluid particles experience levels of loss intermediate between these two extremes.

Equation (29) reveals clearly the three physical processes responsible for the change of subcooling of a fluid particle. Expansion (the second term on the right-hand side) increases subcooling, whereas condensation (the first term) and dissipation (the term involving η) both diminish it. Heat transfer to the surrounding fluid operates in either direction depending on the sign of $(h-h_\infty)$. Expansion takes place within each blade passage but is not operative in the inter-blade and interstage gaps (figure 8). Dissipation may occur everywhere (i.e. both inside and outside the blade passages), but its magnitude depends on the value of η and, hence, the particular pathline followed by the fluid particle. Condensation does not start until an appreciable number of nuclei are formed which, depending on the expansion rate, requires subcoolings of the order of 30–40 K. However, once the Wilson point is reached, condensation occurs continuously and, as shown by equation (27), its rate is directly proportional to the local value of ΔT.

For the illustrative example discussed here, zero equilibration due to turbulent diffusive processes is assumed, i.e. $\tau_E \to \infty$. Figure 9 then shows the calculated variation of the vapour subcooling ΔT associated with the two extreme cases of zero and maximum dissipation. The subcooling of the fluid particles change as a result of the competing effects of the three physical processes described above. Consider first the case of the fluid particle suffering no dissipation (dotted line in figure 9). Here, one of the mechanisms for altering the subcooling, i.e. dissipation, is absent. The fluid particle is superheated (negative ΔT) at the turbine inlet. Its subcooling increases in each blade row because of expansion but remains almost constant between the rows. It attains the Wilson point in the stator of the fifth stage and subsequently experiences an exponential decrease in ΔT owing to the extremely rapid liberation of latent heat. ΔT increases significantly again in the last rotor where the expansion rate is too high to be offset by the counteracting effect of condensation. Much the

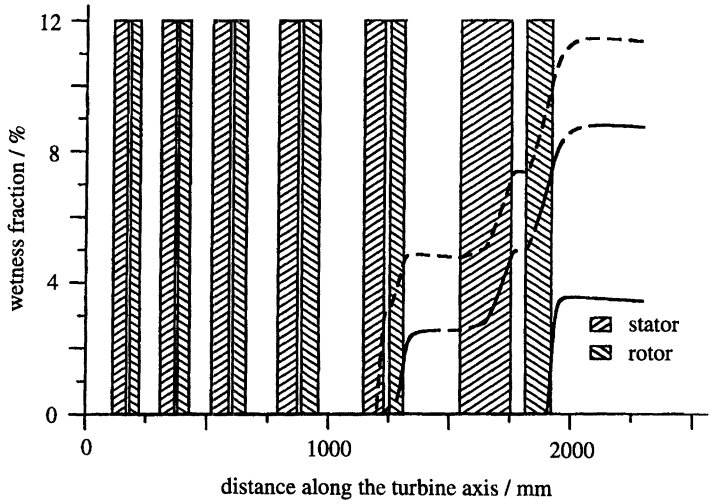

Figure 10. Axial variation in the Ansaldo turbine of the computed wetness fraction showing the limiting cases of zero (– – –) and maximum dissipation (——) and the time-averaged behaviour of all fluid particles (— — —).

same history is repeated for the fluid particle experiencing the maximum loss (plotted as a solid line in figure 9). Here, however, dissipation opposes the increase of the subcooling throughout the flow field. Consequently, the Wilson point occurs much further downstream (in the rotor of the last stage). Other fluid particles, experiencing intermediate amounts of dissipation, attain their Wilson points at locations between the two extremes. The region of nucleation thus covers (in a randomly unsteady manner) almost two complete turbine stages as opposed to being restricted to a very narrow zone in a specific blade row.

Figure 10 shows the axial variation of the wetness fraction for the two limiting cases discussed above and also the time-averaged variation, obtained by averaging the results for all fluid particles (10^4 in total). The time-averaged variation indicates a gradual reversion to equilibrium encompassing four blade rows. This behaviour is in keeping with experimental measurements of wetness using optical techniques but cannot be predicted by conventional steady-state theories of condensation.

The location of the Wilson point has a great effect on the average size of liquid droplets nucleated within each fluid particle. An increase in expansion rate results in an increased subcooling (and hence nucleation rate) at the Wilson point and therefore an increased number density of nuclei. Because reversion to equilibrium always occurs at about the same wetness level (3–4%), the average diameter of the fully developed droplets is smaller, the higher the expansion rate. Although the absolute value of the Wilson point pressure also has some effect, a reliable 'rule of thumb' is

Wilson points occurring at locations of higher expansion rate result in small droplets.

(For a monodispersed droplet population, equation (23) shows that, for a fixed value of y, the droplet radius, r, is inversely proportional to the cube root of n.) Figure 11 shows the axial variation of Sauter mean droplet diameter for the two extreme cases under consideration. The fluid particle experiencing maximum dissipation attains the Wilson point in the rotor of the last stage where the expansion rate is very high. Consequently, the diameter of the fully established droplets is only 0.05 μm, compared with 0.8 μm for the fluid particle suffering no dissipation. The variable

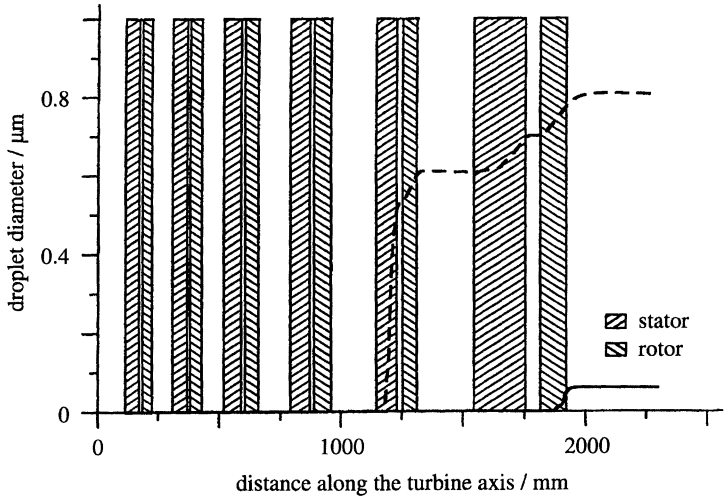

Figure 11. Axial variation in the Ansaldo turbine of the computed Sauter mean droplet diameters for the limiting cases of zero (– – –) and maximum (——) dissipation.

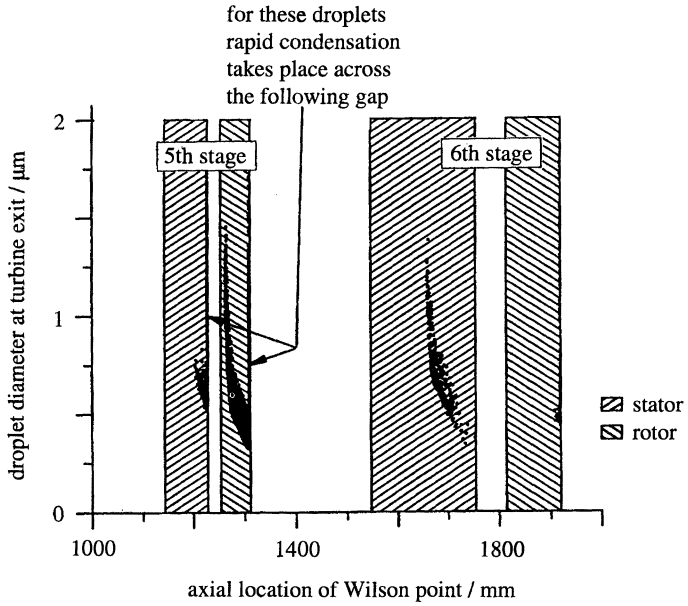

Figure 12. Computed Sauter mean droplet diameter at Ansaldo turbine outlet as a function of the axial location of the Wilson point for all fluid particles.

location of the Wilson point therefore results in large variations in mean droplet diameter. Note, however, that the mean droplet diameters in the two limiting cases do not necessarily represent the extreme limits of droplet size produced in the machine. The droplet size is dependent on the local expansion rate which does not vary monotonically with distance between the extreme locations of the Wilson points.

Figure 12 shows the location of the Wilson points for all the particles considered (10^4). Each point on this diagram corresponds to an individual fluid particle. The

abscissa indicates the axial location of the Wilson point, the ordinate the mean diameter of droplets within the fluid particle on its arrival at the turbine outlet. (Note that each fluid particle is actually composed of a polydispersed distribution of droplet sizes, details of which, although retained by the computational procedure, cannot be included in a single diagram such as figure 12.) It can be seen that the majority of fluid particles nucleate either in the fifth-stage rotor or in the sixth-stage stator. (The absence of Wilson points in the first part of the sixth-state stator results from the very low expansion rate there; see figure 8.) In each blade row, the mean diameter of the droplets becomes progressively smaller as the Wilson point moves towards the trailing edge, because the rate of expansion tends to increase monotonically to each blade throat. Of particular interest, however, are those fluid particles that reach the trailing-edge plane with subcoolings and nucleation rates which, although moderately high, are still insufficient to cause complete reversion to equilibrium. For these particles, the trailing edge marks the Wilson point (i.e. the cessation of nucleation) even if comparatively few droplets have yet been produced. Reversion to equilibrium then occurs within the following gap by condensational growth on existing droplets. Because there is plenty of time available and because the droplet number density is low, these droplets may grow to very large sizes as shown in figure 12. Such fluid particles are then prime candidates for secondary nucleations in succeeding blade rows because their liquid surface area is insufficient to offset (by condensation) the opposing effect of increased subcooling due to the rapid expansion.

An imaginary probe with unlimited resolution in space and time, sited at the turbine outlet, would register the complete droplet size distribution for each fluid particle it encounters. Real probes based on the measurement of attenuated or scattered light, however, record only sufficient information to deduce, at most, the time-averaged droplet size distribution (and sometimes only the time-averaged Sauter mean diameter). To compare the theoretical predictions with such measurements, a theoretical time-averaged droplet size distribution may be constructed at any axial location in the turbine if the diameters and number density of droplets in all the 10^4 fluid particles considered are recorded by the computer for subsequent processing. The calculated time-averaged droplet size distribution for the Ansaldo turbine at outlet is shown in figure 13. The spectrum is polydispersed and highly skewed (i.e. there is a large difference between the mean and most probable diameters) and resembles the shape of similar spectra measured in real turbines (figure 1). This is very significant, as no existing steady-flow calculation procedure can predict such a high degree of polydispersion.

Unfortunately, no measurement of the droplet size distribution is available for the Ansaldo turbine, although the time-averaged Sauter mean diameter has been measured by Walters (1991). This is shown as a function of blade height in figure 14. The measured Sauter mean diameter at mid-span is about 0.4 μm, which is a little smaller than the calculated value of 0.55 μm, shown in figure 13. However, allowing for the uncertainties in the calculation scheme, the level of agreement is extremely encouraging. Of course, many more experimental comparisons are required before it is possible to assert conclusively that the important physical processes are being successfully modelled by the theory in this paper.

All calculations presented in figures 9–13 are based on the assumption that $\tau_E \to \infty$, signifying no equilibration due to turbulent diffusive processes. However, although a realistic value of τ_E is difficult to deduce, it is interesting to conduct a parametric

PHILOSOPHICAL TRANSACTIONS OF THE ROYAL SOCIETY A MATHEMATICAL, PHYSICAL & ENGINEERING SCIENCES

Figure 13

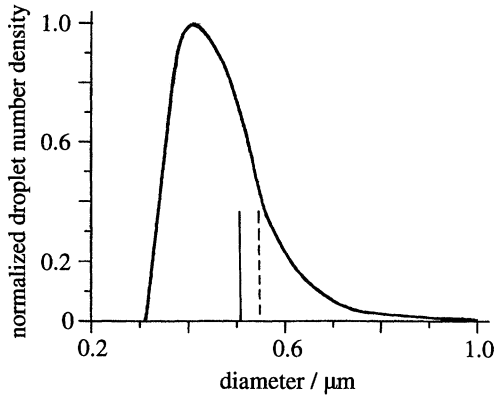

Figure 14

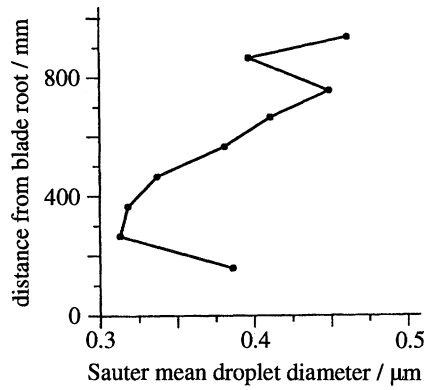

Figure 13. Computed time-averaged droplet size distribution at outlet of the Ansaldo turbine. —— mass mean; –– Sauter mean.

Figure 14. Experimentally measured variation of the Sauter mean droplet diameter at the outlet of the Ansaldo turbine. (Courtesy of P. T. Walters, National Power Technology and Environmental Centre, Leatherhead, U.K.)

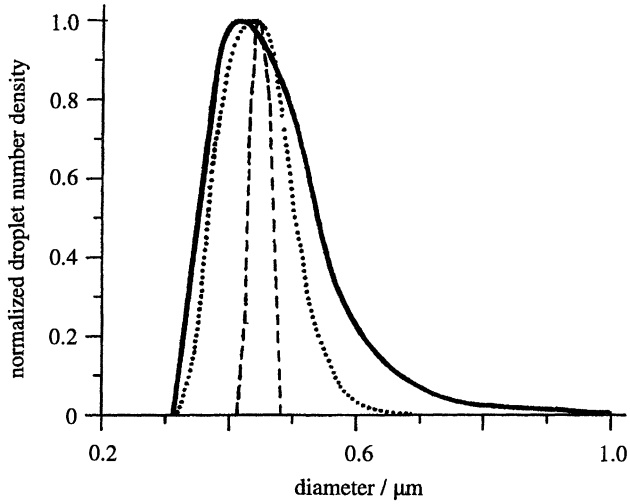

Figure 15. The effect on the computed time-averaged droplet size distribution at outlet from the Ansaldo turbine of varying the equilibration time τ_E. —— $\tau_E \to \infty$, Sauter mean = 0.55 μm; ····· $\tau_E = \Delta t$, Sauter mean = 0.46 μm; –– $\tau_E = 0.1\ \Delta t$, Sauter mean = 0.45 μm.

study on this variable in order to gauge its importance. Figure 15 depicts the time-averaged droplet spectra calculated for three different values of τ_E (i.e. 0.1 Δt, Δt and $\tau_E \to \infty$, where Δt is the residence time of a fluid particle in the final stage stator blade passage). As expected, decreasing values of τ_E representing faster equilibration, produce narrower droplet spectra with smaller mean diameters. The case of $\tau_E \to 0$, implying an infinitely rapid equilibration, can be extrapolated from these calculations. This corresponds to a single specific location of the Wilson point for all fluid particles and results in an almost monodispersed droplet population. This is the result that steady-flow calculation methods based on time-averaged flow properties would compute. Obviously a great deal of the physics of the nucleation process is lost in such time-averaging procedures.

PHILOSOPHICAL TRANSACTIONS OF THE ROYAL SOCIETY A MATHEMATICAL, PHYSICAL & ENGINEERING SCIENCES

Figure 16

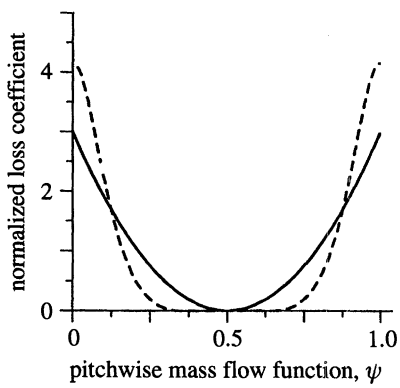

Figure 17

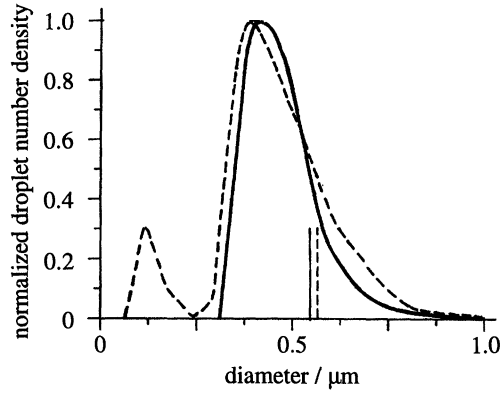

Figure 16. Comparison of the two pitchwise loss profiles used for analysing the Ansaldo turbine. —— profile A; –– profile B.

Figure 17. The effect on the computed time-averaged droplet size distribution at outlet from the Ansaldo turbine of varying the pitchwise loss profiles. —— loss profile A; –– loss profile B. Vertical lines show the Sauter mean diameter of the respective spectra.

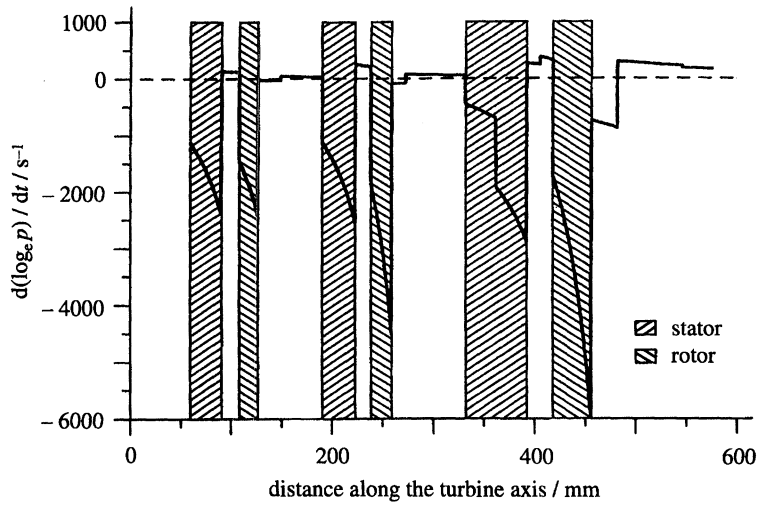

Figure 18. Axial variation of the rate of expansion ($-\dot{p}$) in the three-stage turbine.

An important component of the calculations is the specification of the pitchwise loss profile. To investigate the sensitivity of the results to variations in profile shape, similar calculations were made for the Ansaldo turbine with a loss profile having the same total dissipation of 8% per blade row, but a different shape as shown in profile B of figure 16. The resulting time-averaged droplet size distribution at turbine outlet is shown in figure 17, where, for convenience, the spectrum of figure 13 is included. It is evident that, although the general features of the distributions are similar (including the mean diameters), the actual details depend quite significantly on the shape of the loss profiles. In particular, the proliferation of very small droplets (significant in number but not in mass) associated with loss profile B is due to a shift of the nucleation to a region of higher rate of expansion.

Fluctuations in static temperature due to wake segmentation is a multistage phenomenon. With increasing number of stages, the range of accumulated dissipation

PHILOSOPHICAL TRANSACTIONS OF THE ROYAL SOCIETY A MATHEMATICAL, PHYSICAL & ENGINEERING SCIENCES

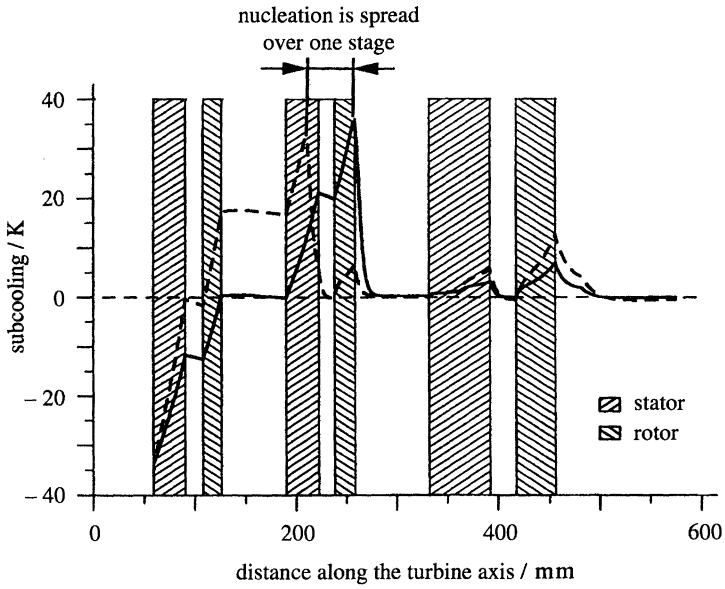

Figure 19. Axial variation in the three-stage turbine of the computed vapour subcooling for the limiting cases of zero dissipation (----) and maximum dissipation (——).

in the different fluid particles increases and the amplitude of the fluctuations becomes greater. It is therefore to be expected that the number of stages in a machine should have a significant effect on the time-averaged droplet spectrum. To investigate this aspect of the theory, another turbine, having only three stages was analysed. Details of the turbine geometry and the calculations are not reproduced here but can be found in Guha (1990). The variation of the expansion rate through the turbine, again calculated by the streamline curvature method, is plotted in figure 18. Figure 19 shows the calculated variation of subcooling for the two extreme cases of fluid particles suffering zero and maximum dissipation respectively. A direct result of the smaller amplitude of fluctuations in this three-stage machine (compared with those in the six-stage Ansaldo turbine) is that the nucleation is spread over just one stage compared with two in the Ansaldo turbine.

The time-averaged droplet size distribution at turbine outlet (based on a parabolic pitchwise loss profile and zero equilibration, $\tau_E \to \infty$) is presented in figure 20. It can be seen that the spectrum exhibits a wide band of droplet sizes, not found in steady calculations, but is much less skewed compared with the distribution computed for the Ansaldo turbine. The three-stage turbine, on average, has a higher expansion rate (figure 18) than the Ansaldo turbine (figure 8). Consequently, the mean diameter of the droplets produced in the former is less than that in the latter. This result agrees with the rule of thumb stated earlier. It also suggests that improved agreement between computed and measured mean droplet diameters might be obtained if blade-to-blade pressure variations were modelled in the calculation.

Another interesting prediction of the theory emerges if the droplet mass (rather than number density) distribution is examined. Figure 21 shows this distribution for the three-stage turbine. A small bimodality can be observed at a droplet diameter of about 0.6 μm. These large size droplets originate from fluid particles where nucleation is terminated, not by the condensational growth of existing nuclei, but by the rapid

Figure 20

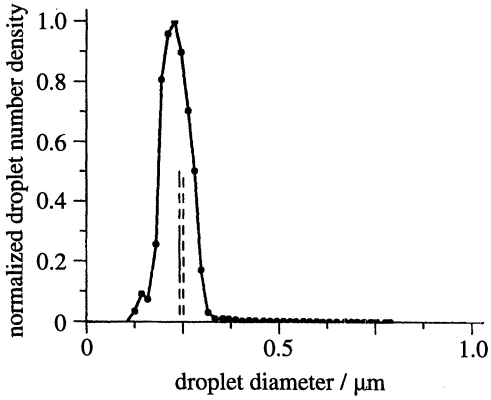

Figure 21

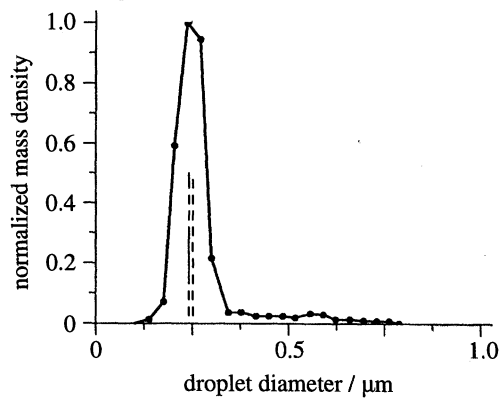

Figure 20. Computed time-averaged droplet number distribution at outlet of the three-stage turbine. —— mass mean; – – – Sauter mean.

Figure 21. Computed time-averaged droplet mass distribution at outlet of the three-stage turbine. —— mass mean; – – – Sauter mean.

decrease in expansion rate at the blade trailing-edge as described above. Experimental measurements of bimodal distributions (with a secondary peak at droplet diameters around 1 μm) have been reported in the literature. The theory therefore offers a possible explanation for the physical mechanism responsible for the creation of droplets of this size.

5. Conclusions

A theory has been developed for predicting the effect of temperature fluctuations on the homogeneous nucleation and growth of water droplets in multistage steam turbines. The fluctuations result from the segmentation of blade wakes by successive blade rows and the amplitude of the fluctuations increases with the number of stages. True turbulent fluctuations (due to shear-layer unsteadiness, etc.) are probably less important and are ignored. For illustrative purposes, the theory has been used to predict the formation of the liquid phase in a six-stage, low pressure turbine, the geometry of which is available in the open literature. An approximation to the pressure field was first obtained by a conventional streamline curvature throughflow calculation in the meridional plane. A Lagrangian viewpoint was then adopted and calculations of phase change were performed for a large number of individual fluid particles negotiating this pressure field on the central streamsurface. The time-averaged behaviour of the condensation process could then be constructed by statistical averaging.

According to the model, the mechanics of nucleation in multistage turbines are quite different from the predictions of conventional steady-state theories of phase change. For example, the nucleation zone may encompass (in a randomly unsteady manner) several blade rows (as opposed to being isolated at a particular position in a specific blade row). The inherent unsteadiness of the process also results in a highly skewed, polydispersed time-averaged droplet size distribution with similar characteristics to spectra measured in real turbines. The comparatively large Sauter mean diameter calculated for the Ansaldo turbine is in reasonable agreement with optical measurements made in the same machine.

PHILOSOPHICAL TRANSACTIONS OF THE ROYAL SOCIETY A MATHEMATICAL, PHYSICAL & ENGINEERING SCIENCES

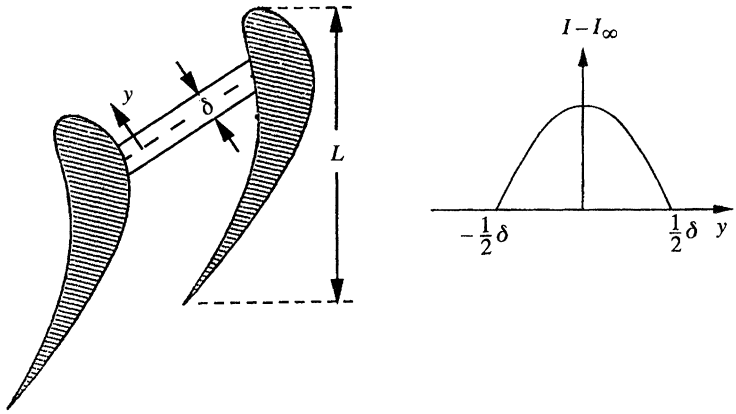

Figure 22. Specification of wake geometry.

The polydispersity and skewness of the droplet spectra increases with increasing number of stages. Sometimes the model predicts a small bimodal distribution resulting from droplets nucleated within the inter-blade and interstage gaps. This is also a characteristic of some experimental measurements.

Calculations show that the time-averaged droplet spectra are comparatively insensitive to the distribution of loss in the streamwise direction but quite sensitive to changes in the pitchwise loss profiles and the equilibration time constant τ_E. These parameters are difficult to specify realistically and more work is required to establish suitable models which accurately reflect these aspects of flow behaviour in real machines. At present, the calculation procedure neglects any circumferential variation of pressure within the blade passages. Because nucleation is so dependent on the rate of expansion experienced by the fluid particles, blade-to-blade variations in pressure probably exert a strong influence on the time-averaged droplet size distribution. It is therefore important to develop techniques for approximating the cascade-plane pressure field without the necessity of undertaking a major computational exercise.

Despite the approximations of the model, we believe the analysis has demonstrated the dominant importance of static temperature fluctuations in the formation and growth of water droplets in multistage steam turbines. The precise details of the processes involved should become clearer as more experimental measurements of droplet size distributions in turbines become available.

We thank Professor J. D. Denton of the Whittle Laboratory, University of Cambridge for the use of his streamline curvature throughflow computer program and Mr P. T. Walters, formerly of the National Power Technology and Environmental Centre, Leatherhead, for supplying the experimental droplet size measurements.

Appendix A. Turbulent diffusion in a wake

The following is a very approximate analysis of the rate at which gradients of relative stagnation enthalpy due to the passage of wakes are eroded by molecular and turbulent diffusive processes. With reference to figure 22, it is assumed that the wake of width δ is convected through the blade passage without distortion and attains the mean flow velocity in the streamwise direction. Any drift towards the suction surface is ignored. It is also assumed that the eddy viscosity μ_t is constant within the wake

PHILOSOPHICAL TRANSACTIONS OF THE ROYAL SOCIETY A MATHEMATICAL, PHYSICAL & ENGINEERING SCIENCES

and the turbulent Prandtl number is unity. Adopting a coordinate system moving with the wake and measuring y as shown in figure 22, equation (14) takes the form

$$\frac{\partial I}{\partial t} = \frac{(k+k_t)}{\rho c_p}\frac{\partial^2 I}{\partial y^2} = \frac{(\mu+\mu_t)}{\rho}\frac{\partial^2 I}{\partial y^2}. \tag{A 1}$$

Assuming, for simplicity, that the rothalpy variation in the y direction is cosinusoidal with period 2δ, the solution of (A 1) is

$$(I-I_\infty) = (I_1-I_\infty)\exp(-t/\tau_E)\cos(\pi y/\delta), \tag{A 2}$$

where I_1 is the rothalpy on the wake centre-line at blade inlet $t = 0$, and

$$\tau_E = \rho c_p \delta^2/\pi^2(k+k_t) = \rho\delta^2/\pi^2(\mu+\mu_t). \tag{A 3}$$

If L is the axial chord-length of the blade and Δt is the transit time of the wake, then

$$\tau_E = \left(\frac{\delta}{\pi L}\right)^2 \frac{Re}{1+(\mu_t/\mu)}\Delta t, \tag{A 4}$$

where $Re = \rho\bar{V}_x L/\mu$ is the Reynolds number based on the mean axial velocity $\bar{V}_x$. Taking $Re = 10^6$, $\delta/L = 0.05$ and $\mu_t/\mu = 50$, gives $\tau_E \approx 5\,\Delta t$. The analysis therefore suggests that rothalpy differences are attenuated by about 20% per blade row.

Equation (A 1) can, of course, be solved for an arbitrary initial wake profile in terms of a Fourier integral but the net result (as long as $t < 0.5\,\tau_E$) is simply to alter slightly the value of the constant in (A 4). Given the approximate nature of the analysis (and particularly the neglect of the major influence of wake distortion due to convective effects), the extra complication cannot be justified.

References

AGARD 1981 Throughflow calculations in axial turbomachines. AGARD-AR-175.

Bakhtar, F. & Alubaidy, A. K. 1984 On the solution of supersonic blade-to-blade flows of nucleating steam by the time-marching method. In *Proc. Instn mech. Engrs conf. 'Computational methods in turbomachinery'*, Birmingham, paper C82/84, pp. 101–111.

Bakhtar, F. & Heaton, A. V. 1988 An examination of the effect of 'wake chopping' on droplet sizes in steam turbines. In *British Nuclear Energy Society, int. conf. 'Technology of turbine plant operating with wet steam'*, London, paper 25, pp. 197–200. London: Thomas Telford.

Denton, J. D. 1978 Throughflow calculations for transonic axial flow turbines. *Trans. Am. Soc. mech. Engrs, J. Engng Pwr*, **100**, 212–218.

Filippov, G. A., Saltanov, G. A. & Ignat'evskii, E. A. 1970 Analysing the condensation of supersaturated steam in turbine stages. *Thermal Engng*, **17**, 26–31.

Guha, A. 1990 The fluid mechanics of two-phase vapour-droplet flow with application to steam turbines. PhD dissertation, University of Cambridge.

Guha, A. & Young, J. B. 1991 Time-marching prediction of unsteady condensation phenomena due to supercritical heat addition. In *Proc. Instn Mech. Engrs European conf. 'Turbomachinery: Latest developments in a changing scene'*, London, paper C423/057, pp. 167–177. Mechanical Engineering Publications Ltd.

Gyarmathy, G. 1962 Bases of a theory for wet steam turbines. Bulletin 6, Inst. Thermal Turbomachines, Federal Technical University, Zurich (CEGB translation 3017).

Gyarmathy, G. & Spengler, P. 1974 Flow fluctuations in multistage thermal turbomachinery. Traupel-Festschrift, Juris-Verlag, Zürich, pp. 95–141 (CEGB translation 17551).

Kerrebrock, J. L. & Mikolajczak, A. A. 1970 Intra-stator transport of rotor wakes and its effect on compressor performance. *Trans. Am. Soc. Mech. Engrs, J. Engng Pwr*, **92**, 359–368.

Kuo, K. 1986 *Principles of combustion*. New York: Wiley.

Lyman, F. A. 1992 On the conservation of rothalpy in turbomachines. In *Am. Soc. mech. Engrs* '*Int. gas turbine and aeroengine congress*', Cologne, paper 92-GT-217.

Skillings, S. A., Moore, M. J., Walters, P. T. & Jackson, R. 1988 A reconsideration of wetness loss in LP steam turbines. In *British Nuclear Energy Society, Int. conf.* '*Technology of turbine plant operating with wet steam*', London, paper 21, 171–177. London: Thomas Telford.

Steltz, W. G., Lee, P. K. & Lindsay, Jr., W. T. 1983 The verification of concentrated impurities in low-pressure steam turbines. *Trans. Am. Soc. mech. Engrs, J. Engng Pwr*, **105**, 192–198.

Walters, P. T. 1973 Optical measurement of water droplets in wet steam. *Instn. Mech. Engrs*, Conf. Warwick, Paper C32/73. *Wet Steam* **4**, 32–40.

Walters, P. T. 1988 Improving the accuracy of wetness measurements in generating turbines by using a new procedure for analysing optical transmission data. *British Nuclear Energy Society, Int. conf.* '*Technology of turbine plant operating with wet steam*', London, paper 27, 207–215.

White, A. J. 1992 Condensation in steam turbine cascades. PhD dissertation, University of Cambridge.

Wood, N. B. 1973 Flow unsteadiness and turbulence measurements in the low-pressure cylinder of a 500 MW steam turbine. In *Proc. Instn. mech. Engrs, Conf. Publication 3*, paper C54/73, 115–121.

Young, J. B. 1982 The spontaneous condensation of steam in supersonic nozzles. *Physico-chem. Hydrodyn.* **3**, 57–82.

Young, J. B. 1984 Semi-analytical techniques for investigating thermal non-equilibrium effects in wet steam turbines. *Int. J. Heat Fluid Flow*, **5**, 81–91.

Young, J. B. 1992 Two-dimensional non-equilibrium wet-stream calculations for nozzles and turbine cascades. *Trans. Am. Soc. mech. Engrs, J. Turbomachinery*, **114**, 569–579.

Young, J. B. & Guha, A. 1991 Normal shock-wave structure in two-phase vapour-droplet flows. *J. Fluid Mech.* **228**, 243–274.

Received 7 December 1992; accepted 15 November 1993

PHILOSOPHICAL TRANSACTIONS OF THE ROYAL SOCIETY A MATHEMATICAL, PHYSICAL & ENGINEERING SCIENCES